

# X-rays from the barred galaxy NGC 4303

D. Tschöke<sup>1</sup>, G. Hensler<sup>1</sup>, and N. Junkes<sup>2</sup>

<sup>1</sup> Institut für Theoretische Physik und Astrophysik, Universität Kiel, 24098 Kiel, Germany (tschoeke@astrophysik.uni-kiel.de)

<sup>2</sup> Max-Planck-Institut für Radioastronomie, Auf dem Hügel 69, 53121 Bonn, Germany

Received 20 March 2000 / Accepted 21 June 2000

**Abstract.** The late-type galaxy NGC 4303 (M61) is one of the most intensively studied barred galaxies in the Virgo Cluster. Its prominent enhanced star formation throughout large areas of the disk can be nicely studied due to its low inclination of about 27°.

We present observations of NGC 4303 with the ROSAT PSPC and HRI in the soft X-ray (0.1–2.4 keV). The bulk of the X-ray emission is located at the nuclear region. It contributes more than 80% to the total observed soft X-ray flux. The extension of the central X-ray source and the  $L_X/L_{H\alpha}$  ratio point to a low luminous AGN (LINER) with a circumnuclear star-forming region. Several separate disk sources can be distinguished with the HRI, coinciding spatially with some of the most luminous H II regions outside the nucleus of NGC 4303. The total star formation rate amounts to 1–2  $M_\odot \text{ yr}^{-1}$ . The X-ray structure follows the distribution of star formation with enhancement at the bar-typical patterns.

The best spectral fit consists of a power-law component (AGN and HMXBs) and a thermal plasma component of hot gas from supernova remnants and superbubbles. The total 0.1–2.4 keV luminosity of NGC 4303 amounts to  $5 \times 10^{40} \text{ erg s}^{-1}$ , consistent with comparable galaxies, like e.g. NGC 4569.

**Key words:** galaxies: individual: NGC 4303 – galaxies: starburst – galaxies: active – X-rays: galaxies

## 1. Introduction

Barred galaxies constitute a major fraction of all disc galaxies classified in the optical, more than 50% including strong bars and intermediate morphologies (Sellwood & Wilkinson 1993). This fraction increases when also near-infrared images are used for classification, thus underlining the importance for the general understanding of the evolution of galaxies. The non-axisymmetric potential has a strong impact on the gas dynamics and the star formation in barred systems. Observations reveal a correlation between the radial abundance gradient and the strength of the bar (Martin & Roy 1994; Friedli et al. 1994; Martinet & Friedli 1997). This is interpreted as the result of two effects caused by the bar: a stronger radial gas flow and hence a stronger radial mixing of metals and the efficiency of star forma-

tion. The radial mass transfer concentrates gas near the galactic center and at the ends of the bar at corotation. Enhanced star formation is the consequence of gas accumulation. The rotating bar potential also heats up the outer disk parts which leads to larger stellar velocity dispersions and a radial diffusion of stars. (Sellwood & Wilkinson 1993).

Galactic bars have also been considered to support the central infall of gas to feed a central “monster” (e.g. Beck et al. 1999). Several authors have claimed that active galactic nuclei (AGN) are more likely in barred galaxies than in non-barred ones (e.g. Simkin et al. 1980; Arsenault 1989). Hummel et al. (1990) note that the fraction of central radio sources in barred spirals is by a factor of 5 higher than in non-barred spirals. Other authors doubt that there is a significantly higher number of bars in galaxies harboring an AGN (e.g. Balick & Heckman 1982; Ho et al. 1997). It appears that the concentration of gas on a scale of  $\sim 1$  kpc at the galactic center required to enhance the central star formation can easily be achieved by a bar potential. It seems much more difficult, however, to accumulate enough gas on a scale of a few pc to tens of pc in order to produce an AGN. Other effects depending on the environment of the galaxies (interaction: Elmegreen et al. 1990; H I contents: Cayatte et al. 1990) play an important role in mass distribution, gas flow, and therefore in the formation and evolution of bars and the star formation history in these systems.

One of the most famous, closest and most widely studied barred galaxies is NGC 4303 (M61), member of the Virgo Cluster, which is observed at an inclination of 27° (Guhathakurta et al. 1988). Optical spectra of this galaxy indicate that it consists of a nuclear starburst and a LINER or Seyfert 2 nucleus (Filippenko & Sargent 1986; Kennicutt et al. 1989; Colina et al. 1997; Colina & Arribas 1999, hereafter CA99). Indications for a high star formation rate (SFR) in NGC 4303 are given by the numerous H II regions (Hodge & Kennicutt 1983; Martin & Roy 1992, hereafter MR92) and three observed supernovae (van Dyk 1992). It also shows strong radio emission distributed over the entire disk (Condon 1983). Colina et al. (1997) and CA99 discussed the question of a starburst–AGN connection in this barred galaxy, using optical spectroscopy and HST UV images. The data range from a nuclear spiral structure of massive star-forming regions with an outer radius of 225 pc down to the unresolved core of a size  $\leq 8$  pc. From the UV data it is not clear if the core is a massive stellar cluster or a pure AGN.

Send offprint requests to: D. Tschöke

VLA observations (Cayatte et al. 1990) show that NGC 4303 is not highly H I deficient, which can be explained by only slight environmental influences in the outermost region of the Virgo Cluster. The projected distance to M87 is 8:2 (Warmels 1988). No significant difference of the abundance gradient in the disk of NGC 4303 compared to non-barred spiral galaxies has been observed (MR92). Martinet & Friedli (1997) discussed the abundance gradient slope in terms of bar age. According to them, a steep gradient in the bar and a flat one in the outer disk are typical for a young bar while a single flat gradient in bar and disk characterizes an old bar. MR92 did not determine the gradient at large radii because of a small number of H II regions. Martinet & Friedli (1997) also claimed that bars in late-type spirals with enhanced star formation like NGC 4303 are expected to be young.

Probable interaction companions are the nearby galaxies NGC 4303 A (Condon 1983) and NGC 4292 (Cayatte et al. 1990), at distances of 7:5 northwest and 10' northeast, respectively.

## 2. Observations and data reduction

In this paper we present data from the High Resolution Imager (HRI) and the Position Sensitive Proportional Counter (PSPC) on board of the X-ray satellite ROSAT. This X-ray telescope was operating in the energy range of 0.1–2.4 keV. For details concerning ROSAT and its detectors see the ROSAT User's Handbook (Briel et al. 1996).

### 2.1. HRI

We proposed HRI pointed observations of NGC 4303 (ROSAT sequence number 600854, PI: N. Junkes), which were carried out in the time periods July 2–8, 1996, June 9–23, 1997, and January 6–7, 1998 with integration times of 16055 sec, 27538 sec, and 5600 sec, respectively (see Table 2). All three observations are centered on RA(2000) = 12<sup>h</sup>21<sup>m</sup>55<sup>s</sup>.2; Dec(2000) = +04°28'11".5.

The three photon lists were combined to create one single image. The data were analyzed using the commercial interactive data language software package IDL (Interactive Data Language). All presented images contain pixel values with units of counts per pixel and second. The images were corrected for vignetting but not for background. To quantify any source counts three circular source-free fields with radii of 49", 34", and 39", respectively, were selected to determine the background level (Table 2). The averaged background flux amounts to  $3.52 \times 10^{-7}$  cts s<sup>-1</sup> arcsec<sup>-2</sup>.

Fig. 1 shows the HRI field of view (FOV) of the three combined data sets, convolved with a Gaussian of 5" FWHM. For reasons of identification the 5 $\sigma$  sources detected with a maximum likelihood method are numbered in Fig. 1 and listed in Table 3. Several single source detections (no. 9–13) coincide with optical peaks in the galaxy. Source no. 18 can be identified as the QSO 1219+044, which served as the central source of the PSPC pointed observation used for spectral anal-

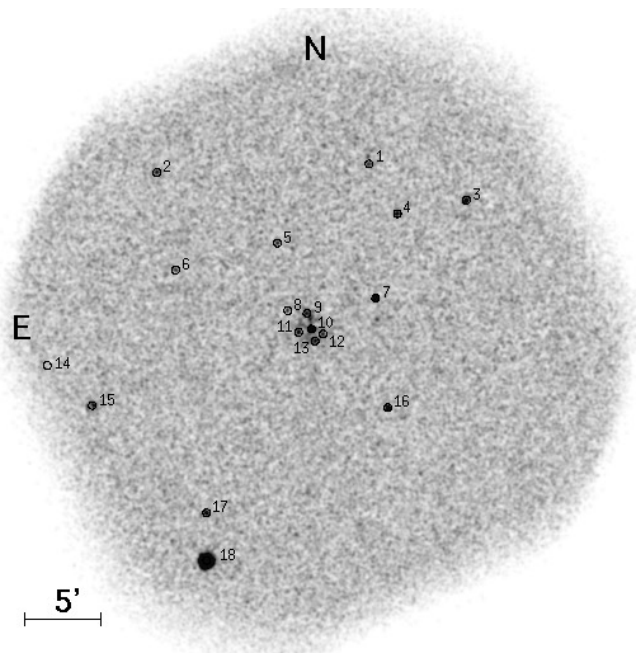


**Fig. 1.** Total field of view of the combined ROSAT HRI observation of NGC 4303. The detected 5 $\sigma$  sources are labeled with numbers. The sources in the center (nos. 9–13) correspond to NGC 4303.

**Table 1.** Some basic parameters of NGC 4303.

	NGC 4303	Reference <sup>a</sup>
alternative name	M61	
	IRAS 12194+0444	
type	SAB(rs)bc	1
RA (2000)	12 <sup>h</sup> 21 <sup>m</sup> 54 <sup>s</sup> .9	2
Dec (2000)	+04°28'25"	2
distance	16.1 Mpc	3
$D_{25}$ diameter	5:9	4
axis ratio	0.97	4
inclination	27°	5
log $L_B$	10.53 <sup>b</sup>	4
log $M_H$	9.71 <sup>b</sup>	4

<sup>a</sup> References: 1) de Vaucouleurs et al. (1991)

2) NASA/IPAC Extragalactic Database

3) Ferrarese et al. (1996)

4) Tully (1988)

5) Guharthakurta et al. (1988)

<sup>b</sup> Corrected for a distance of 16.1 Mpc.

ysis in Sect. 2.2. Source no. 7 coincides spatially with the QSO 1219+047 (Bowen et al. 1996). It turned out that the source is variable the X-rays. Its flux increased by a factor of 3 between the second and third HRI observation (June 1997 and January 1998).

### 2.2. PSPC

Since there exist no particular PSPC observations pointed on NGC 4303, we use ROSAT observations from the archive (ROSAT sequence number 701095, PI: R. Staubert). NGC 4303

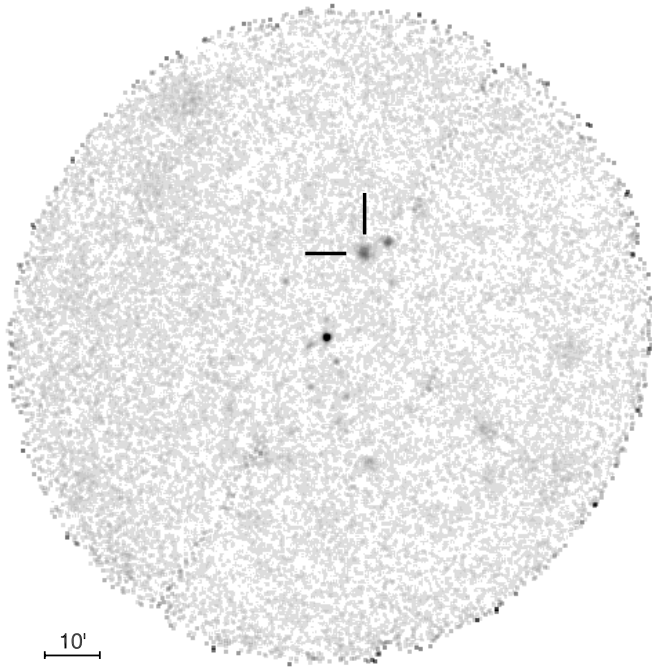
**Table 2.** Date, integration time, and source and background count rates of the HRI and PSPC observations.

	Date	Integration time [s]	Count rate [cts s <sup>-1</sup> ]	Background [cts s <sup>-1</sup> arcsec <sup>-2</sup> ]
HRI	July 2–8, 1996	16055	$8.8 \times 10^{-3}$ <sup>a</sup>	$3.52 \times 10^{-7}$ <sup>a</sup>
	June 9–23, 1997	27538		
	January 6–7, 1998	5600		
PSPC	December 24–26, 1992	8135	0.062	$5.14 \times 10^{-7}$

<sup>a</sup> Combined HRI observations

**Table 3.** EXSAS source detection of X-ray sources in the HRI coinciding with the optical image of NGC 4303.

Source no.	RA (2000)	Dec (2000)	Count rate [10 <sup>-4</sup> cts s <sup>-1</sup> ]	Identification
1	12 <sup>h</sup> 21 <sup>m</sup> 39 <sup>s</sup> .8	+04°39'17"	12.5±2.4	
2	12 <sup>h</sup> 22 <sup>m</sup> 35 <sup>s</sup> .7	+04°38'44"	16.5±2.9	
3	12 <sup>h</sup> 21 <sup>m</sup> 14 <sup>s</sup> .1	+04°36'54"	26.1±3.0	GSC 00285-00416
4	12 <sup>h</sup> 21 <sup>m</sup> 32 <sup>s</sup> .3	+04°36'01"	13.5±2.1	unidentified optical point source
5	12 <sup>h</sup> 22 <sup>m</sup> 03 <sup>s</sup> .9	+04°34'06"	6.4±1.4	
6	12 <sup>h</sup> 22 <sup>m</sup> 30 <sup>s</sup> .7	+04°32'19"	7.9±1.7	
7	12 <sup>h</sup> 21 <sup>m</sup> 38 <sup>s</sup> .0	+04°30'28"	47.2±3.2	QSO 1219+047; variable
8	12 <sup>h</sup> 22 <sup>m</sup> 01 <sup>s</sup> .2	+04°29'40"	5.3±1.3	
9	12 <sup>h</sup> 21 <sup>m</sup> 56 <sup>s</sup> .1	+04°29'29"	10.8±2.0	NGC 4303
10	12 <sup>h</sup> 21 <sup>m</sup> 54 <sup>s</sup> .9	+04°28'27"	36.1±3.0	NGC 4303
11	12 <sup>h</sup> 21 <sup>m</sup> 58 <sup>s</sup> .3	+04°28'15"	8.5±1.6	NGC 4303
12	12 <sup>h</sup> 21 <sup>m</sup> 51 <sup>s</sup> .8	+04°28'08"	6.9±1.5	NGC 4303
13	12 <sup>h</sup> 21 <sup>m</sup> 54 <sup>s</sup> .0	+04°27'40"	11.9±2.0	NGC 4303
14	12 <sup>h</sup> 23 <sup>m</sup> 04 <sup>s</sup> .4	+04°26'03"	29.4±5.1	
15	12 <sup>h</sup> 22 <sup>m</sup> 52 <sup>s</sup> .6	+04°23'26"	28.8±3.5	
16	12 <sup>h</sup> 21 <sup>m</sup> 34 <sup>s</sup> .8	+04°23'17"	21.8±2.3	
17	12 <sup>h</sup> 22 <sup>m</sup> 22 <sup>s</sup> .5	+04°16'23"	18.8±2.8	
18	12 <sup>h</sup> 22 <sup>m</sup> 22 <sup>s</sup> .5	+04°13'16"	351.6±9.2	QSO 1219+044

**Fig. 2.** Total field of view of the ROSAT PSPC observation around the QSO 1219+044. The position of NGC 4303 at an off-axis distance of 17' is marked.

lies in the FOV at an off-axis distance of 17' which is still within the inner part of the supporting ring structure of the telescope. The position of the X-ray counterpart of NGC 4303 is given in Fig. 2. The central source is the QSO 1219+044 (no. 18 in Fig. 1). The image has been convolved with a Gaussian of 25'' FWHM. Due to strong asymmetry and broadening of the point spread function (PSF) with radial distance from the optical axis ( $\sim 25''$  FWHM for an on-axis point source at 1 keV;  $\sim 67''$  FWHM for a 17' off-axis point source at 1 keV; Hasinger et al. 1994) we cannot get any useful spatial information from the PSPC data.

This PSPC exposure was carried out between December 24 and 26, 1992, with an integration time of 8135 sec. The background flux was determined from three circular source-free areas in the field with radii of 83'', 88'', and 75'' and amounts to  $5.14 \times 10^{-7}$  cts s<sup>-1</sup> arcsec<sup>-2</sup>. To analyze the PSPC data we used IDL and the software package XSPEC (Arnaud 1996) for interactively fitting X-ray spectra.

For NGC 4303, we adopt the same distance as of M100, the brightest spiral in the Virgo Cluster (16.1 Mpc; Ferrarese et al. 1996). Then the resolution of the ROSAT detectors of  $\sim 5''$  full width at half maximum (FWHM) for the HRI and  $\sim 67''$  FWHM for the PSPC at an off-axis distance of 17' scale to 390 pc and 5.3 kpc, respectively.

**Table 4.** X-ray sources spatially coinciding with the optical galaxy NGC 4303. The source designations refer to Fig. 3.

Source	RA (2000)	Dec (2000)	Count rate [ $10^{-4}$ cts s $^{-1}$ ]	Source area [arcsec $^2$ ]	Flux <sup>a</sup> (0.1–2.4 keV) [ $10^{-14}$ erg s $^{-1}$ cm $^2$ ]	Luminosity (0.1–2.4 keV) [ $10^{38}$ erg s $^{-1}$ ]
A	12 <sup>h</sup> 21 <sup>m</sup> 54 <sup>s</sup> .5	+04°29′38″	3.4±1.1	200	1.4±0.5	4.3±1.5
B	12 <sup>h</sup> 21 <sup>m</sup> 56 <sup>s</sup> .3	+04°29′28″	9.9±1.8	531	4.1±0.8	12.7±2.5
C	12 <sup>h</sup> 21 <sup>m</sup> 55 <sup>s</sup> .3	+04°29′03″	5.9±1.4	290	2.5±0.6	7.8±1.9
D	12 <sup>h</sup> 21 <sup>m</sup> 58 <sup>s</sup> .3	+04°28′14″	8.9±1.7	380	3.7±0.7	11.5±2.2
E	12 <sup>h</sup> 21 <sup>m</sup> 51 <sup>s</sup> .7	+04°28′08″	7.5±1.5	315	3.1±0.6	9.6±1.9
F	12 <sup>h</sup> 21 <sup>m</sup> 53 <sup>s</sup> .9	+04°27′43″	8.7±1.7	383	3.6±0.7	11.2±2.2
nucleus	12 <sup>h</sup> 21 <sup>m</sup> 55 <sup>s</sup> .5	+04°28′28″	43.9±3.5	1321	87.8±7.0	272±21

<sup>a</sup> Energy conversion factor ECF: disk sources A–F, ECF= $2.4 \times 10^{10}$  cts cm $^2$  erg $^{-1}$ ; nucleus, ECF= $5 \times 10^{13}$  cts cm $^2$  erg $^{-1}$

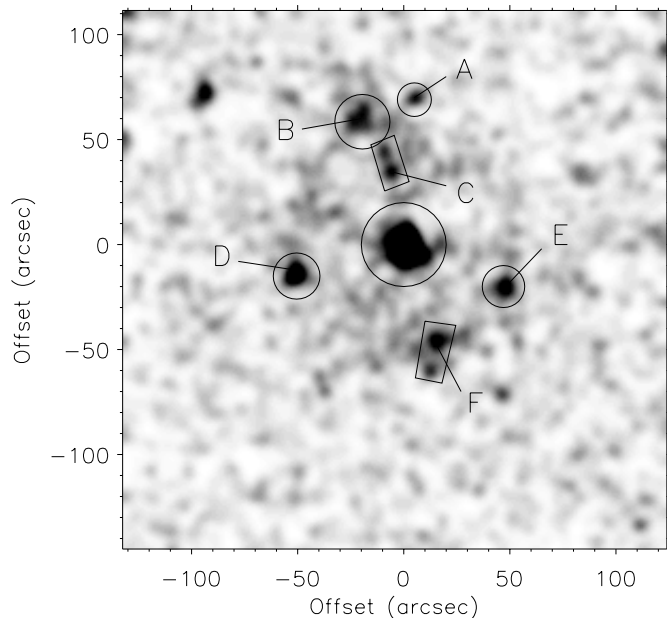


**Fig. 3.** The inner 4′ of the pointed HRI observation. The labeled sources (A–F) are the ones spatially coinciding with the optical disk of NGC 4303 (see text and Table 4 for details). The image is centered on the coordinates of the pointed observation. The distances on the axes are relative to the central X-ray source with the coordinates  $\alpha(2000) = 12^{\text{h}}21^{\text{m}}55^{\text{s}}.5$ ;  $\delta(2000) = +04^{\circ}28′28″.5$ . North is up, east is to the left.

### 3. Results

#### 3.1. Spatial analysis

As already mentioned, no useful spatial information on the X-ray structure of NGC 4303 can be obtained from the PSPC data due to the spatial resolution of the detector, and moreover to the 17′ off-axis position of the source in the FOV.

In contrast, the more detailed HRI image reveals a number of X-ray sources distributed over the galactic disk (Fig. 4). In comparison to the numbered sources in Fig. 1 the closer view allows to distinguish more details. For example, source no. 9 in Fig. 1 splits into three X-ray spots (labeled A–C in Fig. 3). The most luminous source coincides with the center of NGC 4303 and dominates in the soft X-rays. The count rates and fluxes derived for sources from the HRI are listed in Table 4. The cor-

responding areas are plotted in Fig. 3. To determine the fluxes we used the energy conversion factor (ECF) from the ROSAT *Call For Proposals* documentation. The ECF determines the ratio between count rates and unabsorbed source flux in the ROSAT band for given spectral parameters. For the disk sources A–F we assume a 0.3 keV Raymond-Smith model (Raymond & Smith 1977) with an absorption column density of  $3 \times 10^{20}$  cm $^{-2}$ . For the nucleus a power law with  $\Gamma=2.6$  and a column density of  $3 \times 10^{20}$  cm $^{-2}$  (see Sect. 3.2 and Table 5) is applied as spectral model.

The contours of sources B, C, D, and F in Fig. 3 are all located within the optical arm structure and coincide with bright H $\alpha$  emission regions within the spiral arms (Fig. 4). In addition, source E is embedded in the faint outer part of the southwestern spiral arm. MR92 distinguished 79 H II regions in NGC 4303, mainly in the spiral arms. The X-ray contour overlay over the H $\alpha$  image in Fig. 4 reveals that the X-ray sources B, C, D, and F coincide with H II regions, while sources A and E are located near such regions.

Gas dynamical models of barred galaxies (Englmaier & Gerhard 1997) show strong gas accumulation at the tips of the bars due to corotation of the bar structure with the disk what should lead to enhanced star formation. H I observations as well as the existence of prominent H $\alpha$  features strikingly support the outcome of these models. The X-ray contours B and F seem to arise from these regions. The X-ray maximum D is connected with another interesting feature of NGC 4303: in the eastern part the galactic arm seems to be deformed to a boomerang-like bow where source D lies at the bend but without any significant brightening in H $\alpha$ .

The lower X-ray contours of the nucleus indicate a possible extended source. Recent high-resolution UV observations of the central region with the Hubble Space Telescope reveal a spiral-shaped structure of massive young (2–3 Myr) star-forming regions with an outer radius of 225 pc (CA99). This structure cannot be resolved by HRI. Due to the low age of the star clusters almost no thermal X-ray emission is expected at the galactic nucleus (see Sect. 4). The extended X-ray contours may originate from additional sources at distances of about 1 kpc around the nucleus.

No X-ray emission has been detected from the possible interaction companions NGC 4303 A and NGC 4292.

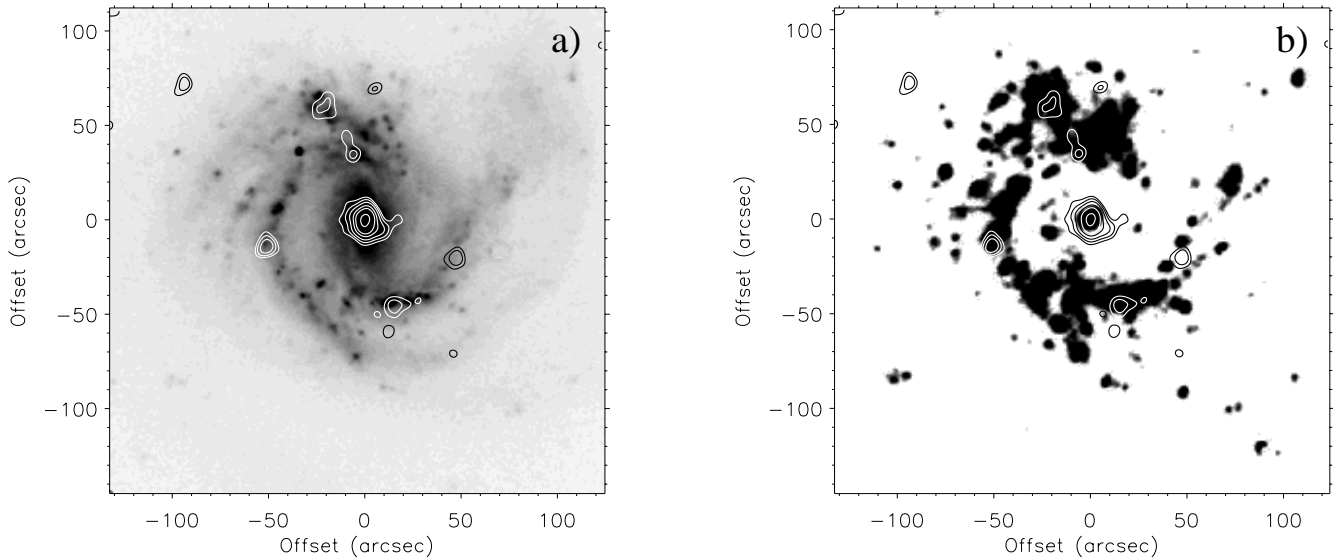


**Fig. 4a and b.** Overlay of the HRI X-ray contours onto the optical image of NGC 4303 **a** taken from Frei et al. (1996) and the H $\alpha$  image **b** taken from MR92. The contour levels are at 5, 7, 10, 15, 20, and 30 $\sigma$  above the mean background with  $\sigma = 1.5 \times 10^{-7}$  cts s $^{-1}$  arcsec $^{-2}$ . The images are centered on the coordinates of the pointed observation. The axis scales are relative to the central X-ray maximum at coordinates  $\alpha = 12^{\text{h}}21^{\text{m}}55^{\text{s}}.5$ ;  $\delta = +04^{\circ}28'28''.5$ . North is up, east is to the left.

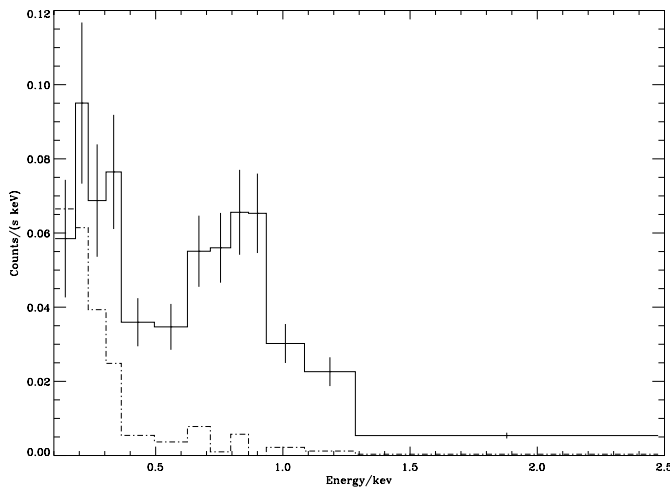


**Fig. 5.** Background-subtracted ROSAT PSPC spectrum of NGC 4303 in the energy range of 0.1–2.4 keV. The 505 photons were binned to get a signal-to-noise ratio of 6. The dashed-dotted line represents the contribution of the background (see text).

### 3.2. Properties of the X-ray spectrum

Since the HRI maxima are separated by only 50'', and because of the reasons mentioned in Sect. 2.2, the PSPC observations do not allow to study the spectra of the X-ray components of NGC 4303 individually. ROSAT PSPC detected  $505 \pm 24$  background-subtracted source counts from NGC 4303 in a total integration time of 8135 sec. The spectra of the source and the background are shown in Fig. 5.

We fitted the spectrum with several single-component models, as Bremsstrahlung (BS), Raymond-Smith model (RS), and

a power law (PO), and a combined RS-PO model. The results are listed in Table 5.

A single power-law model implies the assumption, that the active nucleus of NGC 4303 dominates the X-ray emission. Furthermore, the sources detected by the HRI in the galactic disk would also have to be described with the same power law. The photon index in this model is  $\Gamma = 3.2 \pm 0.2$ . The emission of an AGN in the ROSAT energy band is best described by a power law with a photon index of  $\Gamma \sim 2.4$ ; nevertheless some cases have been observed with  $\Gamma > 3$  (MCG -5-23-16: Mulchaey et al. 1993; Mkn 335: Turner et al. 1993). High-mass X-ray binaries (HMXB) found in young star-forming regions in the spiral arms have a similar spectral shape in the 0.1–2.4 keV energy range with a photon index of  $\Gamma \sim 2.7$  (Mavromatakis 1993). The column density of the absorbing component amounts to  $5.7 \times 10^{20}$  cm $^{-2}$ , which is by a factor of 3 higher than the Galactic foreground H I column density (Dickey & Lockman 1990, DL90). Nevertheless, self-absorption within NGC 4303 must be expected, and small-scale deviations from the observed Galactic value by DL90 cannot be ruled out and may result in a higher absorption from the Milky Way. The resulting 0.1–2.4 keV X-ray luminosity amounts to  $1.3 \times 10^{41}$  erg s $^{-1}$ . The flux portion from the sources outside the nuclear region as observed with the HRI amounts to  $\sim 1.4 \times 10^{40}$  erg s $^{-1}$  in the case of a single power-law emission model with  $\Gamma = 3.2$  using the corresponding ECF of  $1 \times 10^{10}$  cts cm $^2$  erg $^{-1}$ . Assuming a mean X-ray luminosity of  $10^{37}$  erg s $^{-1}$  for an HMXB, as observed in the Milky Way (Fabbiano et al. 1982; Watson 1990) would require an unlikely high number of 1400 of these systems to produce the observed X-ray flux. The ratio of OB stars to HMXBs is assumed to be  $\sim 500$  (Fabbiano et al. 1982). This means that a total number of  $7 \times 10^5$  OB stars would be required to account for the HMXB

**Table 5.** Best spectral fits to the PSPC data of NGC 4303 and the derived model parameters. For the determination of the X-ray luminosity a distance of 16.1 Mpc is assumed.

Model	$N_{\text{H}}$	$kT$	$\Gamma$	$Z$	Norm	Red. $\chi^2$	d.o.f.	$F_{\text{X}}$	$L_{\text{X}}$
(1)	(2)	(3)	(4)	(5)	(6)	(7)	(8)	(9)	(10)
RS + PO	$3.34^{+1.95}_{-0.39}$	$0.32^{+0.14}_{-0.07}$	$2.6^{+0.2}_{-0.6}$	1	6.2 (RS) 1.5 (PO)	1.3	8	$1.50^{+0.48}_{-0.44}$ ( $0.19^{+0.04}_{-0.01}$ )	$4.7^{+1.5}_{-1.4}$ ( $0.59^{+0.12}_{-0.03}$ )
PO	$5.72^{+0.68}_{-0.50}$		$3.2 \pm 0.2$		2.1	1.4	10	$4.18^{+1.93}_{-0.88}$	$12.9^{+6.0}_{-2.7}$
RS	$2.87^{+0.67}_{-0.53}$	$0.57^{+0.08}_{-0.09}$		0.006	1.4	1.4	9	$1.13^{+0.08}_{-0.10}$	$3.47^{+0.25}_{-0.31}$
BS	$3.19^{+0.53}_{-0.49}$	$0.56^{+0.09}_{-0.07}$			2.5	1.4	10	$1.26^{+0.12}_{-0.10}$	$3.91^{+0.37}_{-0.31}$

Col. (1) – Spectral models: BS = thermal Bremsstrahlung, RS = Raymond-Smith, PO = power law.

Col. (2) – Column density in units of  $10^{20} \text{ cm}^{-2}$ .

Col. (3) – Plasma temperature in units of keV.

Col. (4) – Photon index.

Col. (5) – Metallicity in units of  $Z_{\odot}$ .

Col. (6) – Scaling factor: for BS in units of  $(10^{-18}/(4\pi D^2)) \int n_e n_I dV$ ,  $n_e, n_I$  = electron and ion densities ( $\text{cm}^{-3}$ ); for RS in units of  $(10^{-19}/(4\pi D^2)) \int n_e n_H dV$ ,  $n_e, n_H$  = electron and H densities ( $\text{cm}^{-3}$ ); for PO in units of  $10^{-4}$  photons  $\text{keV}^{-1} \text{ cm}^{-2} \text{ s}^{-1}$  at 1 keV.

Col. (7) – Reduced  $\chi^2$ .

Col. (8) – Degrees of freedom.

Col. (9) – Unabsorbed X-ray flux in units of  $10^{-12} \text{ erg cm}^{-2} \text{ s}^{-1}$ . Values in brackets give the contribution of the thermal component.

Col. (10) – X-ray luminosity in units of  $10^{40} \text{ erg s}^{-1}$ . Values in brackets give the contribution of the thermal component.

X-ray flux in NGC 4303. Even if we consider to have  $10^5$  OB stars in NGC 4303, as observed e.g. in Mkn 297 (Benvenuti et al. 1979), it is still a factor of 7 higher than expected. Moreover, this is the required number only for the disk sources and would involve almost  $1.5 \times 10^7 M_{\odot}$  in massive stars with a Salpeter IMF and, by this, would require a moderately high SFR of about  $15 M_{\odot} \text{ yr}^{-1}$  in the disk. On the other hand, the corresponding supernova type II (SN II) rate ( $0.1 \text{ yr}^{-1}$ ) should contribute to the X-ray emission via hot gas.

The single component models BS and RS show similar results. Consequently, we only achieve an adequate fit of RS with very low metallicity, e.g. the portion of emission lines to the spectrum is very small. In contrast, it is expected that emission lines of highly ionized elements, like Fe and Mg, should play an important role in the X-ray spectrum of SNe II in starburst regions because of the nucleosynthesis of massive SN II progenitor stars (Woosley & Weaver 1985). In both models the column density is about  $3 \times 10^{20} \text{ cm}^{-2}$  and the plasma temperature is 0.6 keV. For the BS model we get a total X-ray luminosity of  $4 \times 10^{40} \text{ erg s}^{-1}$ , for the RS model it is  $3.5 \times 10^{40} \text{ erg s}^{-1}$ . RS models with different higher metallicities yield unacceptable fits.

The fit of the X-ray spectrum with a two-component model (RS+PO) is only slightly better than the one-component fits. Nevertheless, from the points mentioned above and the physical picture discussed in Sect. 4 this model serves as the best explanation for the observed soft X-ray emission. Hydrogen column density ( $N_{\text{H}}=3.3 \times 10^{20} \text{ cm}^{-2}$ ) and power-law spectral index ( $\Gamma=2.6$ ) lie within the expected range (as discussed for the single power law above). The plasma temperature of 0.3 keV fits with the observed values of other galaxies (e.g. NGC 253: Forbes et al. 1999; NGC 1808: Junkes et al. 1995). The total 0.1–2.4 keV luminosity for this model amounts to  $4.7 \times 10^{40} \text{ erg s}^{-1}$

with 13% contribution from the RS component. The spectral fit together with the residuals is plotted in Fig. 6.

#### 4. Discussion

From the quality of the spectral fits alone there is no significance for favoring a single-component model or a combination of two components. Due to the lack of any spatial information in the PSPC image there is no possibility to distinguish between different spatial and spectral components simultaneously. So only the combined information from the PSPC and HRI data allows a more detailed interpretation of the X-ray results.

Several points speak against the single PO component model, as discussed in Sect. 3.2. A more likely scenario is a composition of several different emission sources, like an active nucleus, HMXBs, and supernova remnants (SNRs). In the following we will therefore discuss a composite emission model and the comparison with the UV and optical observations of the galactic core.

##### 4.1. The nucleus of NGC 4303

As can be discerned from the HRI image (Fig. 3 and Table 4), most of the X-ray emission of NGC 4303 (83%) comes from the central region of the galaxy. Three different pictures are imaginable for the nucleus: a central active nucleus, a central or circumnuclear region with enhanced star formation, or a combination of both phenomena. Any of these cases requires a sufficient gas density at the galactic center. This can be achieved by a barred potential which triggers radial gas flow from the outer regions toward the nucleus. On the other hand, from numerical simulations including gas dynamics bar formation has proved to be only a transient phenomenon (Combes 2000). In this pic-

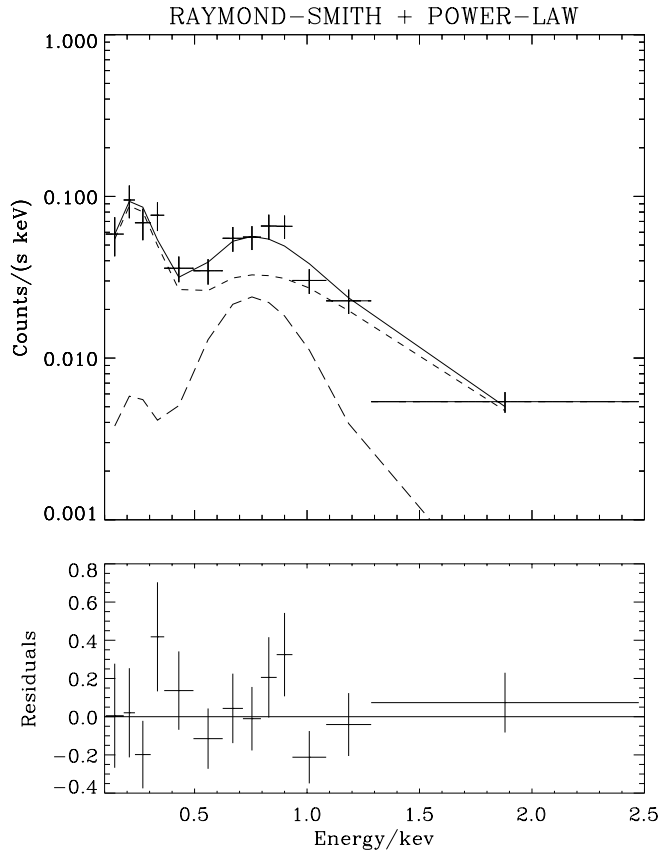


**Fig. 6.** Fit of the observed ROSAT PSPC spectrum of NGC 4303 with the two-component model RS+PO (solid line). The parameter values for this model are listed in Table 5. The long-dashed line shows the spectrum of the thermal model component, the short-dashed line represents the power-law component. The residuals of the fit are plotted in the lower box.

ture, the galactic bar will be destroyed by the gas inflow after only a few cycles. A new bar-phase can follow this gas infall due to a subsequent gravitational instability from the accreted central mass. The problem with this picture is the contradiction of a necessary gas inflow to form and feed any nuclear activity (starburst and/or AGN) and the fact that this gas inflow destroys the bar. It seems that a sufficiently massive black hole can provide for its fuelling (Fukuda et al. 1998). Another efficient way for gas to flow further into the center is a second smaller bar embedded into the first one due to a second inner Lindblad resonance (Friedli & Martinet 1993). In some cases, a gaseous circumnuclear ring is formed at the end of the second bar.

The concentrated X-ray emission from the galactic core in NGC 4303 may originate from an AGN and/or a nuclear or circumnuclear starburst. A starburst can contribute in two different ways to the X-ray flux. First, the produced star population contains HMXBs, emitting an X-ray radiation in spectral shape similar to an AGN. HMXBs cannot be distinguished from AGN in the ROSAT data. Additionally, high-mass stars (above  $\sim 8$ – $10 M_{\odot}$ ) evolve to SNe II at an age of  $\sim 10^7$  yr, depending on their initial mass. The SNe II from one star cluster form a cumulative expanding superbubble filled with hot gas which can be

described by a thermal Bremsstrahlung spectrum and additional emission lines and recombination edges of highly ionized heavy elements produced in high-mass stars and released by their SN II explosions, e.g. O, Ne, Mg, Si, and Fe. Theoretical models for the spectral emission of such a hot diffuse gas are MEKA (Mewe et al. 1985) and the model by Raymond & Smith (1977), which we used in our spectral fit.

If we apply a two-component model to describe the X-ray spectrum of NGC 4303, the comparison of the flux ratio from the nucleus (83% in the HRI) and the disk sources (17% in the HRI) suggests that the central source can be described by the power-law component (87% in the spectral fit). The thermal RS emission exclusively originates from the disk sources, indicating ongoing star formation. To consider the possible extension of  $\sim 25''$  of the central source, as represented by the lowest contours, it is imaginable that a small fraction of the X-ray flux is emitted by a circumnuclear starburst at a distance of  $\sim 1$  kpc around the core. This would add a thermal component to the non-thermal X-ray nucleus. On the other hand, a fraction of the X-ray flux from the disk sources may come from HMXBs within these star forming regions.

Fuelling an AGN on scales of a few parsec at the center of the galaxy leads to the problem of reducing the angular momentum of the central gas by several orders of magnitude, as dynamical simulations show (Barnes & Hernquist 1991). Concentration of gas in a ring-like feature around the nucleus with a radius of  $\sim 1$  kpc is dynamically much easier to achieve. The HRI image agrees with the picture of an extended X-ray source with a diameter of the order of  $\sim 2$  kpc at the galactic center of NGC 4303, explained by a circumnuclear starburst region with an additional possible compact nuclear source. The discovered massive rotating circumnuclear disk in NGC 4303 can provide by its spiral-like structure of massive star forming regions an effective mechanism to channel gas from the circumnuclear regions further down to the nucleus to feed the AGN. But one has to consider that the spiral structure in the UV has a diameter of only 225 pc, while the extension of the central X-ray source is about 2 kpc in diameter. The spiral feature detected in the UV cannot be resolved with the HRI.

From the analysis of UV and optical magnitudes and colors of the central 250 pc Colina & Wada (2000) estimated ages of 5–25 Myr for the star-forming regions. Consequently a contribution to the central X-ray flux from SNRs and cumulatively expanding hot gas has to be expected. The question remains whether we observe a pure nucleus of massive star-forming clusters or a composition of these star clusters and a low luminous AGN. If NGC 4303 contains a non-thermal active nucleus, the X-ray luminosity of  $4 \times 10^{40}$  erg  $s^{-1}$  points to only a low luminous AGN (LINER). Koratkar et al. (1995) found a correlation between  $L_X$  and  $L_{H\alpha}$  for low luminous AGNs of  $L_X/L_{H\alpha} \approx 14$ . Pérez-Olea & Colina (1996) investigated the correlation between optical and X-ray luminosities of several AGNs with circumnuclear star-forming rings, pure AGNs, and pure starburst galaxies. The pure starbursts in their galaxy sample show  $L_X/L_{H\alpha}$  values of 0.03–0.3, 100 times smaller than for pure AGNs. If we take the  $H\alpha$  luminosity of NGC 4303

derived by Keel (1983) and assume that 10% originate from the nucleus, we get  $\log L_{\text{H}\alpha}(\text{nucleus}) = 39.2$  (adopted for a distance of 16.1 Mpc). Therefore the X-ray-to- $\text{H}\alpha$  ratio amounts to  $\log(L_{\text{X}}/L_{\text{H}\alpha}) = 1.4$ , which agrees with the value found by Koratkar et al. (1995). Even the lower  $L_{\text{X}}$  value from a single RS model ( $\sim 2.5 \times 10^{40} \text{ erg s}^{-1}$  for the nucleus) results in  $\log(L_{\text{X}}/L_{\text{H}\alpha}) = 1.2$ . Typical pure starburst galaxies show  $\text{H}\alpha$  luminosities of the order of their X-ray luminosities or higher.

#### 4.2. The galactic disk

At first glance the optical disk of NGC 4303 seems to have the quite symmetrical morphology of a late-type spiral. A closer look reveals that the eastern spiral arm of the galaxy has a much more prominent form with a boomerang-like shape and a lot more bright emission regions than the western counterpart. The northern disk shows a complex structure with many separate features. This asymmetry is more discernible in the  $\text{H}\alpha$  image. The  $\text{H II}$  regions are mainly located in the northern part of the disk at the junction of the bar with the eastern spiral arm and along that arm. A close encounter of one or both of the nearby galaxies NGC 4303 A and NGC 4292 may have caused these features. The interaction within the Virgo Cluster is another possible source. Infall into the intracluster medium could cause ram pressure effects. Nevertheless, NGC 4303 is located at the outer edge of the cluster, which may produce only a moderate disturbance. This agrees with the  $\text{H I}$  distribution over the whole optical disk. Galaxies lying nearer to the cluster center show  $\text{H I}$  deficiencies and concentration of the neutral hydrogen in the central regions, indicating past interactions with the  $\text{H I}$  gas been stripped off from the outer disk regions.

As a striking indication for accumulation of gas in these regions, the X-ray sources A–C and F within the galactic disk of NGC 4303 are located at the ends of the bar. Gas dynamical simulations of barred galaxies have shown this accumulation due to mass flows along the bar to the center and to the ends of the bar, respectively (Noguchi 1988; Englmaier & Gerhard 1997). The increased densities lead to enhanced star formation.

From the low inclination of NGC 4303 no direct information can be obtained whether the disk is warped or not. But it is striking that source D lies exactly at the bend of the eastern boomerang-shaped arm. This may indicate that this X-ray source is caused by the tidal force leading to a local gas concentration. Another indirect hint for a past interaction comes from the spectra of the QSO 1219+047 (source no. 7 in Fig. 1), a QSO whose line-of-sight penetrates the outer  $\text{H I}$  disk of NGC 4303. Bowen et al. (1996) detected complex  $\text{Mg II}$  absorption, spanning a velocity range of  $\sim 300 \text{ km s}^{-1}$ , despite the low inclined galactic disk. This high velocity is not fully understood. One possible explanation could be the result of interactions between NGC 4303 and the nearby companions.

#### 4.3. Star formation in the disk

Table 4 lists the observed count rates and derived 0.1–2.4 keV luminosities for the single X-ray sources in the disk of NGC 4303.

These include the assumptions of a Raymond-Smith plasma with solar abundances at a temperature of 0.3 keV. A power-law model would increase the values by a factor of 2.5. A rough estimation of the SFR in the disk from the X-ray luminosities is done by calculating the  $\text{SN II}$  rate  $\nu_{\text{SN}}$  using a SNR model by Cioffi (1990), and assuming a Salpeter IMF within a mass interval from  $0.1 M_{\odot}$  to  $100 M_{\odot}$  and with all stars with masses above  $8 M_{\odot}$  evolving to  $\text{SNe II}$ . According to Cioffi, a SNR expanding into an ISM with a density of  $1 \text{ cm}^{-3}$  radiates a total energy of  $4.7 \times 10^{49} \text{ erg}$  in the soft X-ray regime above 0.1 keV for a time of  $\sim 10^4 \text{ yr}$ . Norman & Ikeuchi (1989) investigated the cumulative effect of a number of SNRs. The total SFR in the disk of NGC 4303 from the X-ray luminosity amounts to  $0.5 M_{\odot} \text{ yr}^{-1}$ . This however is just a very simple estimation, containing several simplifications, as e.g. the sum of the single SN model from Cioffi (1990) for several cumulatively expanding SNRs in an evolving OB association, or the derivation of the total disk SFR from single X-ray sources. A more detailed determination of the SFR, for example using an analytic superbubble model by Suchkov et al. (1994), would need information about the extensions and expansion time of the superbubbles, in order to determine the mechanical energy release by the  $\text{SNe II}$  and, by this, the SN rate. This can be compared with the observed X-ray luminosity.

Besides the mentioned restrictions the difference between the SFR estimated from the X-ray flux and the SFR derived by the  $\text{H}\alpha$  flux by Kennicutt (1983) ( $14 M_{\odot} \text{ yr}^{-1}$ ) may be due to several reasons. Kennicutt used a Miller-Scalo IMF which increases the SFR by a factor of about 1.5. The total  $\text{H}\alpha$  luminosity underlies a distance determination with a Hubble constant of  $50 \text{ km s}^{-1} \text{ Mpc}^{-1}$ . Taking a radial velocity of  $1569 \text{ km s}^{-1}$  (de Vaucouleurs et al. 1991) leads to a 3.8 times higher luminosity than taking the distance of 16.1 Mpc which we used. Additionally, the fact that not all  $\text{H II}$  regions may emit an adequate X-ray flux or are not strong enough to be detected lowers the estimated SFR from the X-ray luminosity which implies the existence of high-mass stars having been evolved to  $\text{SNe II}$ . Possible X-ray emission from diffuse hot gas within the disk may lie below the detection limit of  $1.1 \times 10^{-6} \text{ cts s}^{-1} \text{ arcsec}^{-2}$  ( $5\sigma$  above background level). A very faint component located at the spiral arms can be seen in outlines in Fig. 3, but is not detected at a  $3\sigma$  level. This limit corresponds to an X-ray flux of  $4.6 \times 10^{-17} \text{ erg s}^{-1} \text{ cm}^{-2} \text{ arcsec}^{-2}$  (ECF for a RS model as in Table 4). Kennicutt (1983) also admitted to treat the derived  $\text{H}\alpha$  flux and resulting SFR with extreme caution because of only moderate accuracy due to possibly strong extinction effects. The  $\text{H}\alpha$  flux derived by Keel (1983) is by a factor of 30 lower than the one derived by Kennicutt, after adopting the same distance.

Strikingly, the sources B and F both coincide with some of the most  $\text{H}\alpha$  luminous  $\text{H II}$  regions (Sources no.s 27 and 69 with  $\log F_{\text{H}\alpha} = -12.12$  and  $\log F_{\text{H}\alpha} = -11.99$ , respectively, in MR92). Depending on the fraction of the central X-ray flux stemming from SNRs and superbubbles or from an AGN component, the SFR for the core is of the order of  $1 M_{\odot} \text{ yr}^{-1}$ .

## 5. Conclusions

We have analyzed spatial and spectral data from the barred late-type spiral galaxy NGC 4303 in the soft X-ray regime. Several separate X-ray sources can be observed in the core and disk of the galaxy. The locations of the sources correspond to several H II regions and indicate a concentration of gas at the center and at the ends of the galactic bar, in agreement with numerical simulations of gas dynamics in a barred potential.

The low spatial resolution of the PSPC observation of NGC 4303 does not allow a distinction of several individual X-ray sources within the object. The best fit of the soft X-ray spectrum taking into account the information from the high resolution HRI observation is a combination of a RS component with a temperature of 0.3 keV and a power-law component with a spectral index of 2.6. The total 0.1–2.4 keV X-ray luminosity amounts to  $4.7 \times 10^{40}$  erg s<sup>-1</sup>, in agreement with other comparable barred galaxies with a nuclear starburst, like e.g. NGC 4569 (Tschöke et al. in preparation). A pure starburst model for the nucleus of NGC 4303 would require a special explanation for the unusually high  $L_X/L_{H\alpha}$  ratio.

The combination of the flux fraction of the separate sources, the spectral information, and the comparison with the H $\alpha$  luminosity from the core leads to the following picture: the soft X-ray emission originates from a composition of several distinct emission regions. The central source consists of a low luminous AGN and a circumnuclear starburst. The disk sources are dominated by SNRs and superbubbles in star forming regions preferably at the ends of the bar and along the eastern spiral arm. Several HMXBs may contribute to the X-ray flux.

The disk X-ray sources are coincident with some of the most luminous H II regions in the galaxy. The estimated total SFR from the X-ray flux is 1–2 M $_{\odot}$  yr<sup>-1</sup>. Most H II regions are not detectable in the X-ray, like most H $\alpha$  sources in the eastern boomerang-shaped arm. The enhanced star formation in NGC 4303 may have been caused by some kind of interaction although the H I morphology of the galaxy does not support very strong perturbation. If a dwarf galaxy has fallen in and merged with NGC 4303 in the past, the bar may have been produced with the subsequent triggering of the star formation at the center and in the spiral arms. The accreted dwarf galaxy would be resolved and not directly detectable.

*Acknowledgements.* The authors are grateful to Dominik Bomans for stimulating discussions, and to Dr. Olga Sil'chenko for her substantial and constructive report. The ROSAT project is supported by the German Bundesministerium für Bildung, Wissenschaft, Forschung und Technologie (BMBF) and the Max-Planck-Society. This research has made use of the NASA/IPAC Extragalactic Database (NED) which is operated by the Jet Propulsion Laboratory, Caltech, under contract with the NASA. Observations made with the NASA/ESA Hubble Space Telescope were used, obtained from data archive at STScI. STScI is operated by the Association of Universities for Research in Astronomy, Inc. (AURA) under the NASA contract NAS 5-26555.

## References

Arnaud K.A., 1996, *Astronomical Data Analysis Software and Systems V*, ASP Conf. Ser. vol. 101, eds. Jacoby G., Barnes J., p. 17

- Arsenault R., 1989, *A&A* 217, 66  
 Balick B., Heckman T.M., 1982, *ARA&A* 20, 431  
 Barnes J.E., Hernquist L.E., 1991, *ApJ* 370, L65  
 Beck R., Ehle M., Shoutenkov V., Shukurov A., Sokoloff D., 1999, *Nat* 397, 324  
 Benvenuti P., Casini C., Heidmann J., 1979, *Nat* 282, 272  
 Bowen D.V., Blades J.C., Pettini M., 1996, *ApJ* 472, L77  
 Briel U., Aschenbach B., Hasinger G., et al., 1996, *ROSAT User's Handbook* (MPE, Garching)  
 Cayatte V., van Gorkom J.H., Balkowski C., Kotanyi C., 1990, *AJ* 100, 604  
 Cioffi D., 1990, in "Physical Processes in Hot Plasmas", NATO ASI Series C, Vol. 305, eds. Brinkmann W., Fabian A.C., Giovannelli F., Kluwer, Dordrecht, p. 1  
 Colina L., Arribas S., 1999, *ApJ* 514, 637 (CA99)  
 Colina L., García-Vargas M.L., Mas-Hesse J.M., Alberdi A., Krabbe A., 1997, *ApJ* 484, L41  
 Colina L., Wada K., 2000, *ApJ* 529, 845  
 Combes F., 2000, in "Galaxy Dynamics: from the Early Universe to the Present", ASP Conference Series, Vol. 197, eds. Combes F., Mamon G.A., Charmandaris V., p. 15  
 Condon J.J., 1983, *ApJS* 53, 459  
 de Vaucouleurs G., de Vaucouleurs A., Corwin Jr. H.G., et al., 1991, *Third Reference Catalogue of Bright Galaxies*, Springer Verlag, New York  
 Dickey J.M., Lockman F.J., 1990, *ARA&A* 28, 215 (DL90)  
 Elmegreen D.M., Elmegreen B.G., Bellin A.D., 1990, *ApJ* 364, 415  
 Englmaier P., Gerhard O., 1997, *MNRAS* 287, 57  
 Fabbiano G., Feigelson E., Zamorani G., 1982, *ApJ* 256, 397  
 Ferrarese L., Freedman W.L., Hill R.J., et al., 1996, *ApJ* 464, 568  
 Filippenko A.V., Sargent W.L., 1986, in "Structure and Evolution of Active Galactic Nuclei", eds. Giuricin G., Mardirossian F., Mezetti M., Ramella M., Dordrecht: Reidel, p. 21  
 Forbes D.A., Polehampton E., Stevens I.R., Brodie J.P., Ward M.J., 1999, submitted to *MNRAS*, *astro-ph/9908048*  
 Frei Z., Guhathakurta P., Gunn J.E., Tyson J.A., 1996, *AJ* 111, 174  
 Friedli D., Martinet L., 1993, *A&A* 277, 27  
 Friedli D., Benz W., Kennicutt R., 1994, *ApJ* 430, L105  
 Fukuda H., Wada K., Habe A., 1998, *MNRAS* 295, 463  
 Guhathakurta P., van Gorkom J.H., Kotanyi C.G., Balkowski C., 1988, *AJ* 96, 851  
 Hasinger G., Boese G., Predehl P., et al., 1994, *Legacy* 4, 40, MPE/OGIP Calibration Memo CAL/ROS/93-015, Version: 1995, May 8  
 Ho L.C., Filippenko A.V., Sargent W.L.W., 1997, *ApJ* 487, 591  
 Hodge P.W., Kennicutt R.C., 1983, *AJ* 88, 296  
 Hummel E., van der Hulst J.M., Keel W.C., 1990, *A&A* 236, 333  
 Junkes N., Zinnecker H., Hensler G., Dahlem M., Pietsch W., 1995, *A&A* 294, 8  
 Keel W.C., 1983, *ApJS* 52, 229  
 Kennicutt R.C. 1983, *ApJ* 272, 54  
 Kennicutt R.C., Keel W.C., Blaha C.A., 1989, *AJ* 97, 1022  
 Koratkar A., Deustua S.E., Heckman T., et al., 1995, *ApJ* 440, 132  
 Martin P., Roy J.-R., 1992, *ApJ* 397, 463 (MR92)  
 Martin P., Roy J.-R., 1994, *ApJ* 424, 599  
 Martinet L., Friedli D., 1997, *A&A* 323, 363  
 Mavromatakis F., 1993, *A&A* 273, 147  
 Mewe R., Gronenschild E.H.B.M., van den Oord G.H.J., 1985, *A&AS* 62, 197  
 Mulchaey J.S., Colbert E., Wilson A.S., et al., 1993, *ApJ* 414, 144  
 Noguchi M., 1988, *A&A* 203, 259

- Norman C.A., Ikeuchi S., 1989, *ApJ* 345, 372  
Pérez-Olea D.E., Colina L. 1996, *ApJ* 468, 191  
Raymond J.C., Smith B.W., 1977, *ApJS* 35, 419  
Sellwood J.A., Wilkinson A., 1993, *Rep. Prog. Phys.* 56, 173  
Simkin S.M., Su H.J., Schwarz M.P., 1980, *ApJ* 237, 404  
Suchkov A.A., Balsara D.S., Heckman T.M., Leitherer C., 1994, *ApJ* 430, 511  
Tully R.B., 1988, *Nearby Galaxies Catalog*, Cambridge University Press, Cambridge
- Turner T.J., George I.M., Mushotzky R.F., 1993, *ApJ* 412, 72  
van Dyk S.D., 1992, *AJ* 103, 1788  
Warmels R.H., 1988, *A&AS*, 72, 427  
Watson M.G., 1990, in “Windows on Galaxies”, eds. Fabbiano G., Gallagher J.S., Renzini A., Kluwer, Dordrecht, p. 177  
Woosley S.E., Weaver T.A., 1985, in “Radiation Hydrodynamics in Stars and Compact Objects”, *Proc. of the IAU Colloquium No. 89*, eds. Mihalas D., Winkler K.-H., p. 91